Room-temperature high-speed mid-infrared quantum cascade laser with π-shape metal contact

Xu Gao[1], Ke Yang[2], Yi-xuan Zhu[2], Junqi Liu[2], Shenqiang Zhai[2], Shuman Liu[2], Ning Zhuo[2], Jinchuan Zhang[2], Lijun Wang[2], Fengqi Liu[2], Xiao-hua Wang[1], and Zhi-peng Wei[1]

[1]Changchun University of Science and Technology Jilin
[2]Institute of Semiconductors Chinese Academy of Sciences

November 11, 2022

Abstract

We demonstrate a high-speed 8.5 µm quantum cascade laser with room temperature continuous wave operation. The maximum output power of 141 mW is obtained at 20 . The parasitic capacitance of the device is decreased from 36.6 pF to 7.1 pF by monolithic integrating a π-shape metal contact electrode. This results in an increase in the -3 dB RF modulation bandwidth from 870 MHz to 4.5 GHz compared with the conventional electrode configuration.

Room-temperature high-speed mid-infrared quantum cascade laser with π-shape metal contact

Xu Gao[1,2,3], Ke Yang[2,3], Yi-xuan Zhu[2,3], Jun-qi Liu[2,3,], Shen-qiang Zhai[2], Shu-man Liu[2,3], Ning Zhuo[2], Jin-chuan Zhang[2,3], Li-jun Wang[2,3], Feng-qi Liu[2,3,4], Xiao-hua Wang[1,] and Zhi-peng Wei[1,]

[1]State Key Laboratory of High Power Semiconductor Lasers, School of Physics, Changchun University of Science and Technology, Changchun 130022, China

[2]Key Laboratory of Semiconductor Materials Science, Institute of Semiconductors, Chinese Academy of Sciences, Beijing 100083, China

[3]College of Materials Science and Opto-Electronic Technology, University of Chinese Academy of Sciences, Beijing 101408, China

Email: jqliu@semi.ac.cn; biewang2001@126.com; and zpweicust@126.com

We demonstrate a high-speed 8.5 μm quantum cascade laser with room temperature continuous wave operation. The maximum output power of 141 mW is obtained at 20 . The parasitic capacitance of the device is decreased from 36.6 pF to 7.1 pF by monolithic integrating a π-shape metal contact electrode. This results in an increase in the -3 dB RF modulation bandwidth from 870 MHz to 4.5 GHz compared with the conventional electrode configuration.

Introduction: High-speed quantum cascade lasers (QCLs) are essential for a plethora of applications in free-space optical communication (FSOC) [1], high-sensitivity spectroscopy [2], mode-locking [3], etc. Due to the particularity of the transition between subbands, the theoretical modulation bandwidth of QCLs can reach the order of 100 GHz [4]. However, higher electrical parasitics limit the modulation performance of QCLs, various approaches have been proposed to reduce electrical parasitics. Using thicker chalcogenide glass ($Ge_{0.25}Se_{0.75}$) as insulating material to achieve 7 GHz modulation response at 20 K. Single-mode buried grating QCL using thickened SiO_2 as insulating layer achieves a flat frequency response of 3 GHz at room temperature [5]. A frequency response of 15 GHz at 77 K is achieved through the integration of microstrip lines with dielectric laser waveguide [6]. A single-mode distributed feedback (DFB) QCL integrated with a three-terminal microwave coplanar waveguide structure displayed 3-dB bandwidth of up to 6.6 GHz [7]. High-frequency modulation of 3-dB bandwidth at 5.6 GHz achieved by buried heterostructure ultrashort resonator [8]. The RC constant is reduced by inserting a matching printed circuit, and the 3-dB bandwidth is increased from about 0.9 to 2.2 GHz [9]. Although high-speed QCLs have been studied a lot, most of these devices can only operate below room temperature.

In this letter, we propose a room temperature high-speed QCL emitting at 8.5 μ m with the maximum continuous wave (CW) output power of 141 mW at 20 . After optimization of the monolithically integrated π-shape metal contact electrode, a parasitic capacitance is reduced to a very low value of 7.1 pF resulting in a high -3 dB RF-modulation bandwidth of 4.5 GHz.

Design and fabrication: The QCL structure was grown on an n-doped InP substrate by metal-organic chemical vapor deposition (MOCVD) with an active-region (AR) structure similar to Ref. [10]. The layer thicknesses in nanometers, starting from the first injection barrier, are as follows:**4.0** /1.3/**1.0** /5.2/**0.9** /5.1/**1.0** /4.7/**1.6** /3.6/**2.2** /2.9/**1.8** /2.7/**1.9** */2.6/**2.0**/2.4/**2.5**/* 2.5/**3.1** /2.3, where InAlAs barriers are in bold, InGaAs wells in roman, and underlined numbers correspond to the doped layers (Si, 2 × 10^{17}cm^{-3}). The epitaxial layer sequence starting from the InP substrate is as follows: 0.5 μ m InP buffer layer (Si, 1 × 10^{17} cm^{-3}), 3 μ m lowdoped InP cladding layer (Si, 4 × 10^{16} cm^{-3}), 300 nm InGaAs confinement layer (Si, 5 x 10^{16}cm^{-3}), 35 periods InGaAs/InAlAs active structure, 300 nm InGaAs confinement layer (Si, 5 x 10^{16}cm^{-3}), 3.3 μ m low-doped InP cladding layer (Si, 4 × 10^{16} cm^{-3}), 0.4 μ m graded-doped InP layer (Si, 1 × 10^{17}cm^{-3} – 1 x 10^{18}cm^{-3}), and 0.3 μ m InP contact layer (Si, 5 × 10^{18} cm^{-3}).

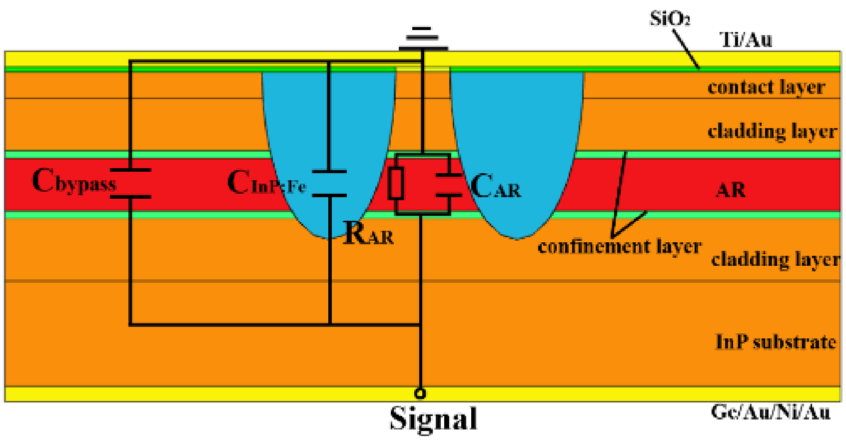

a

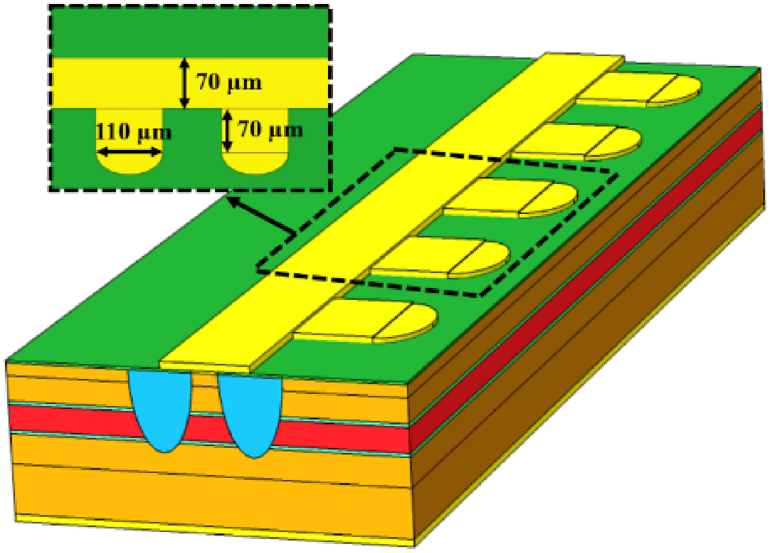

b

Fig. 1 *Device structure diagram.*

a Structure diagram of conventional QCL

b Structural diagram of QCL with π-shape electrode. Inset: The size of π-shape electrode.

The conventional double-channal planar buried heterostructure (BH) device structure is shown in Figure 1a, which is processed into a BH configuration with a ridge width of 10 μ m. The fabrication process is the same as that described in Ref. [10]. For packaging, the chips were soldered epi-up on AlN submounts to improve heat removal efficiency. Then the submounts with chips were mounted on the copper heat sinks with indium solder followed by wire bonding. The parasitic capacitance of the entire device can be roughly composed of three parts: $\hat{}_{\tau o \tau \alpha \lambda} = \hat{}_{\beta \psi \pi \alpha \sigma \varsigma} + \hat{}_{I\nu \Pi:\Phi \epsilon} + \hat{}_{AP} = \epsilon_0 \epsilon_\varsigma \Sigma/\delta$, as shown in the illustration, where ϵ_ς is sheet-permittivity of InP:Fe and AR,S is pumped area, d is thickness of the layer. To reduce bypass capacitance, we skillfully removed the redundant Ti/Au contact around the current injection window through standard photolithography and etching as shown in Figure 1b, only leaving the current injection window portion and enough pad area for bonding wires. The size of the pad is as shown in the illustration, which just meets the size of the gold wire. This makes the metal contact electrode look like π-shape. The whole top electrode area is reduced from 6.8×10^5 μ m^{2}to 2.37×10^5 μ m^2. The processed wafer was cleaved into 2 mm bars, and a high-reflectivity coating consisting of Al_2O_3/Ti/Au/Ti/Al_2O_3(200/10/100/10/120 nm) was applied on the back facet with the front facet left uncoated.

Experiments and discussion: For characteration, the laser was mounted on a holder containing a thermistor combined with a thermoelectric cooler (TEC) to monitor and adjust the sub-mount temperature. The emitted optical power was measured with the calibrated thermopile detector placed in front of the laser facet without any correction. The spectra of devices were tested by a Fourier transform infrared spectrometer with a resolution of 0.25 cm^{-1}.

Figure 2a shows the CW power-current-voltage (P-I-V) characteristics of a QCL with π-shape metal contact electrode at different heat sink temperature and a conventional QCL at 20 °C. The QCL with π-shape metal contact electrode CW output power ranging from 181 mW at 10 °C to 60 mW at 40 °C.

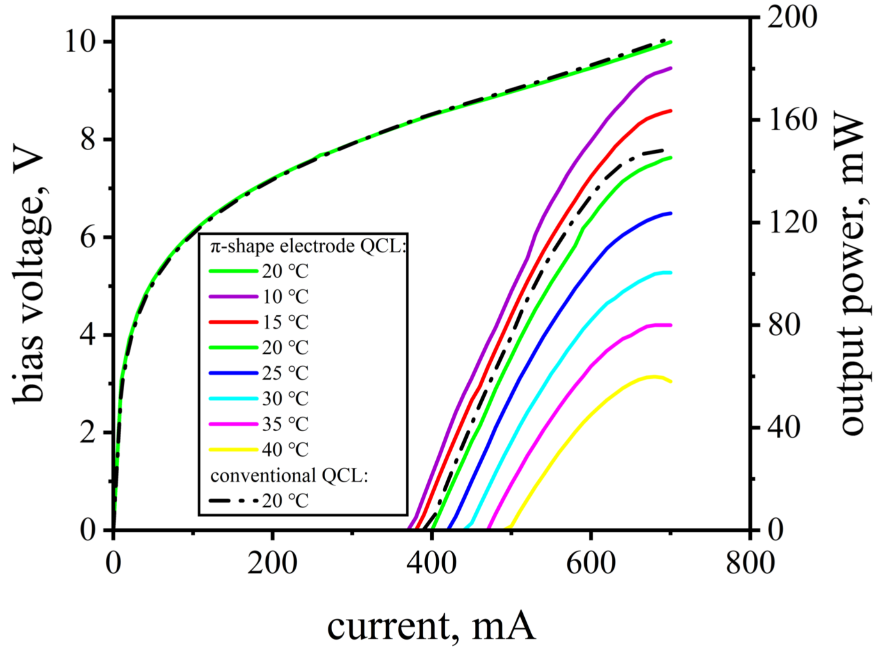

a

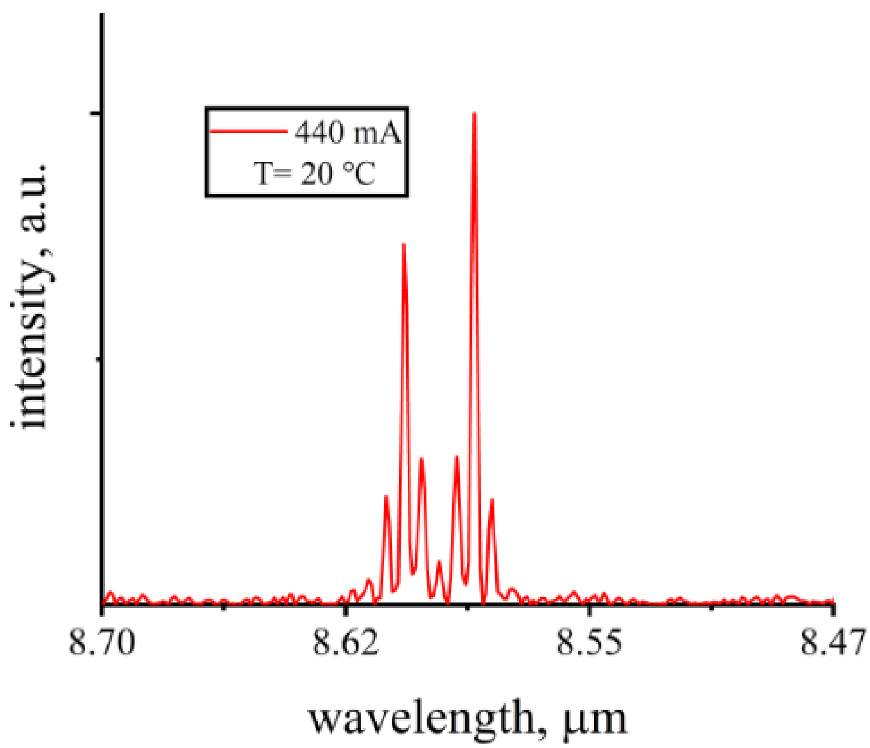

b

Fig. 2 *Ελεςτριςαλ ανδ οπτιςαλ ςηαραςτεριστιςς οφ α ςονεντιοναλ ΧῨΛ ανδ α ΧῨΛ ωιτη π-σηαπε ελεςτροδε δυρινγ ῨΩ οπερατιον.*

a P-I-V characteristics for various heat sink temperatures

b CW spectra for various pumping currents at 20 °C.

At 20 °C, the device exhibited a threshold current of 400 mA and a maximum CW output power of 141 mW. The traditional QCL have a maximum output power of 148 mW. According to the I-V characteristic curve of the device, it can be calculated that the differential resistance above the threshold current is about 5 Ω. Figure 2b we present the CW lasing spectra of the QCLs at 20 °C and the injection current is 440 mA. The device exhibits multimode lasing with a center wavelength around 8.5μ m.

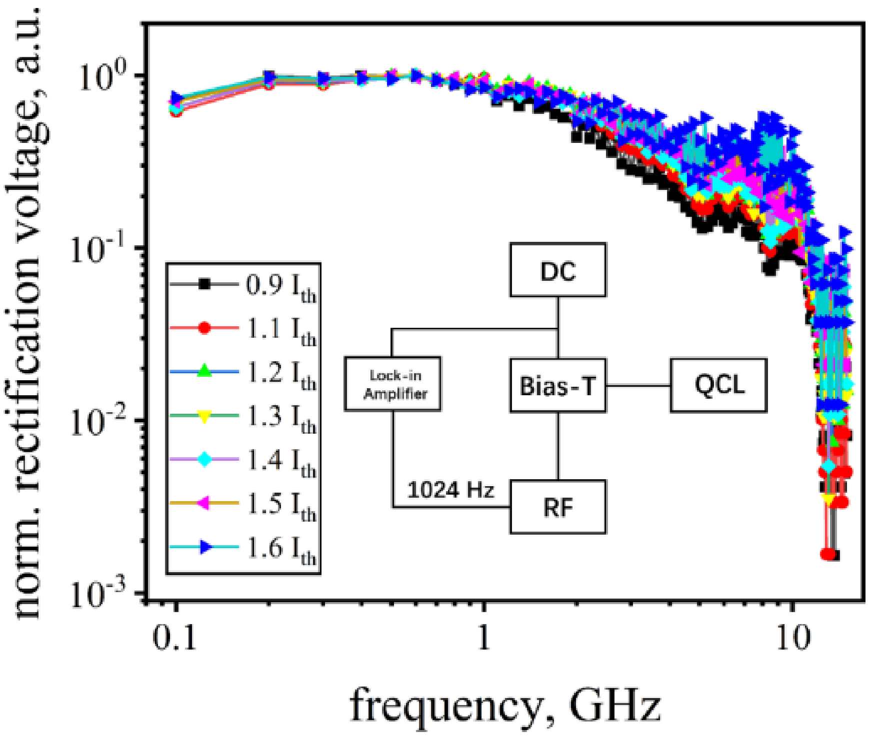

Fig. 3 *Νορμαλιζεδ ελεςτριςαλ ρεςτιφιςατιον δατα οφ α Χ̃Λ ωιτη π-σηαπε ελεςτροδε ατ διφφερεντ βιασ-ςυρρεντς βετωεεν 0.9 $I_{\tau\eta}$ ανδ 1.6 $I_{\tau\eta}$. Ινσετ: Τηε εξπεριμενταλ σετυπ φορ α μιςροωαε ρεςτιφιςατιον μεασυρεμεντ.*

To characterize the high frequency modulation performance of the devices, we applied a microwave rectification technology [11]. The inset of Figure 3 shows a diagram of the experimental setup. In this measurement, a microwave signal and a direct current (DC) bias are injected into the laser through a bias-T. The laser is DC biased at different currents, while the RF power is kept at 10 dBm. An1.024 kHz amplitude modulation is added to the RF generator by an additional arbitrary function generator while sweeping from 100 MHz to 15 GHz in steps of 100 MHz. Figure 3 shows the normalized electrical rectification curves for a QCL with π-shape metal contact electrode measured at widespread driving currents ranging from 0.9 I_{th} (360 mA) to 1.6 I_{th} (640 mA). Further increase in modulation bandwidth with the increasing DC current is observed. It is also in good agreement with literature [6-8], where similar results were obtained above lasing threshold.

Figure 4 shows the comparison results of the normalized electrical rectification data and corresponding fitting results at 1.6 I_{th} of a conventional QCL and a π-shape QCL. As can be seen, the -3 dB bandwidth of the conventional QCL is 870 MHz and the π-shape electrode QCL is 4.5 GHz. By fitting the measured value with the theoretical curve (dashed line) of the rectification model, the corresponding capacitance value can be extracted. It can be obtained that the parasitic capacitance of the conventional structure QCL is 36.6 pF, while the parasitic capacitance of the π-shape electrode QCL is 7.1 pF. The test results show that after integrating a π-shape electrode, the parasitic capacitance of the device is reduced effectively, resulting in an increase of the -3 dB modulation bandwidth from 870 MHz to 4.5 GHz.

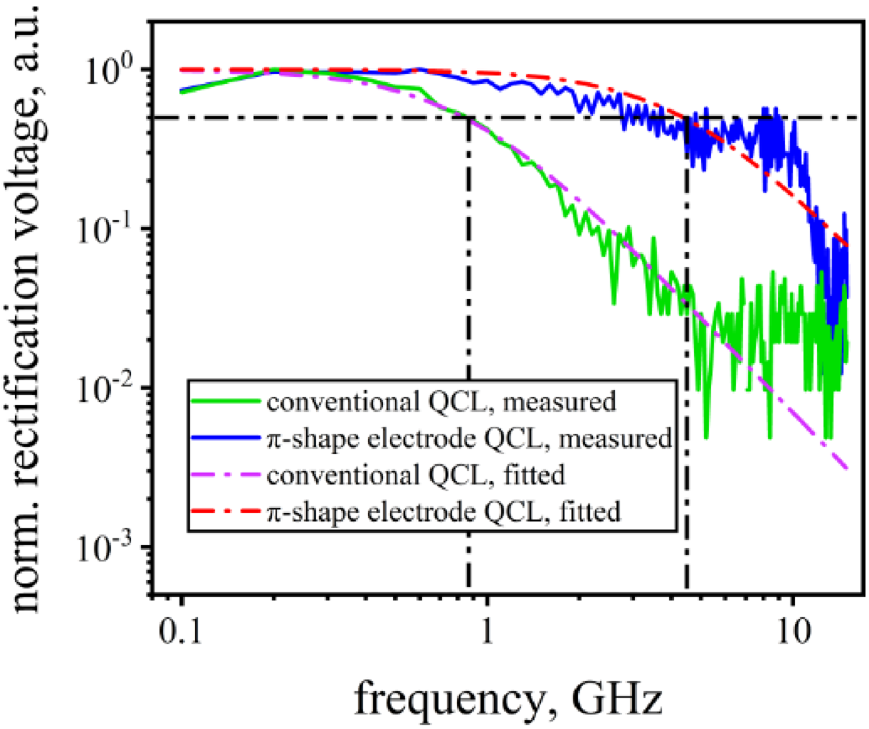

Fig. 4 *Τηε ςομπαρισον ρεσυλτς οφ τηε νορμαλιζεδ ελεςτριςαλ ρεςτιφιςατιον δατα οφ α ςονεντιοναλ Χ˘Λ ανδ α π-σηαπε ελεςτροδε Χ˘Λ.*

Conclusion: We have demonstrated a CW high-speed QCL with emitting wavelength of 8.5μ m and output optical power about 141 mW at 20 . By monolithic integrating a π-shape metal contact electrode, the parasitic capacitance of the device is effectively reduced from 36.6 pF to 7.1 pF and the -3 dB modulation bandwidth is increased from 870 MHz to 4.5 GHz compared with the conventional electrode configuration. The device shows a high application potential in FSOC, active mode locking, etc.

Acknowledgments: This work was supported in part by the National Natural Science Foundation of China under Grant Nos. 61835011, 61991430, and the Key Program of the Chinese Academy of Sciences under Grant Nos. XDB43000000.

References

1. Pang, X., Ozolins, O., Zhang, L., Schatz, R., Udalcovs, A., Yu, X., Jacobsen, G., Popov, S., Chen, J., and Lourdudoss, S., 'Free-Space Communications Enabled by Quantum Cascade Lasers', Phys. Status Solidi A, 2021, 218, (3), p. 2000407.

2. Villares, G., Hugi, A., Blaser, S., and Faist, J., 'Dual-Comb Spectroscopy Based on Quantum-Cascade-Laser Frequency Combs', Nature Communications, 2014, 5, (1), p. 5192.

3. Hillbrand, J., Andrews, A.M., Detz, H., Strasser, G., and Schwarz, B., 'Coherent Injection Locking of Quantum Cascade Laser Frequency Combs', Nature Photonics, 2019, 13, (2), pp. 101-104.

4. Haldar, M.K., 'A Simplified Analysis of Direct Intensity Modulation of Quantum Cascade Lasers', IEEE Journal of Quantum Electronics, 2005, 41, (11), pp. 1349-1355.

5. Zhou, Y.H., Zhai, S.Q., Liu, J., Liu, F., Zhang, J., Zhuo, N., Wang, L., and Wang, Z., 'High-Speed Quantum Cascade Laser at Room Temperature', Electronics Letters, 2016, 52, (7), pp. 548-549.

6. Calvar, A., Amanti, M.I., St-Jean, M.R., Barbieri, S., Bismuto, A., Gini, E., Beck, M., Faist, J., and Sirtori, C., 'High Frequency Modulation of Mid-Infrared Quantum Cascade Lasers Embedded into Microstrip Line', Applied Physics Letters 2013, 102, (18), p. 181114.

7. Hinkov, B., Hugi, A., Beck, M., and Faist, J., 'Rf-Modulation of Mid-Infrared Distributed Feedback Quantum Cascade Lasers', Optics Express, 2016, 24, (4), pp. 3294-3312.

8. Zhou, Y.H., Liu, J.Q., Zhai, S.Q., Zhuo, N., Zhang, J.C., Liu, S.M., Wang, L.J., Liu, F.Q., and Wang, Z.G., 'High-Speed Operation of Single-Mode Tunable Quantum Cascade Laser Based on Ultra-Short Resonant Cavity', AIP Advances, 2021, 11, (1), p. 015325.

9. Yang, K., Liu, J., Zhai, S., Zhang, J., Zhuo, N., Wang, L., Liu, S., and Liu, F., 'Room-Temperature Quantum Cascade Laser Packaged Module at 8 μm Designed for High-Frequency Response', Electronics Letters, 2021, 57, (17), pp. 665-667.

10. Fei, T., Zhai, S.Q., Zhang, J.C., Zhuo, N., Liu, J.Q., Wang, L.J., Liu, S.M., Jia, Z.W., Li, K., Sun, Y.Q., Guo, K., Liu, F.Q., Wang, Z.G., 'High power λ˜ 8.5 μm quantum cascade laser grown by MOCVD operating continuous-wave up to 408 K', Journal of Semiconductors, 2021, 42(11): 112301.

11. Liu, H.C., Jianmeng, L., Buchanan, M., and Wasilewski, Z.R., 'High-Frequency Quantum-Well Infrared Photodetectors Measured by Microwave-Rectification Technique', IEEE Journal of Quantum Electronics, 1996, 32, (6), pp. 1024-1028.